ChemComm

COMMUNICATION

View Article Online
View Journal

Check for updates

Cite this: DOI: 10.1039/d4cc02651a

Received 31st May 2024,
Accepted 4th July 2024

DOI: 10.1039/d4cc02651a

rsc.li/chemcomm

Published on 05 July 2024. Downloaded by Zhejiang University on 7/17/2024 9:55:18 AM.

Ferrocene-modified covalent organic framework for efficient oxygen evolution reaction and CO_2 electroreduction†

Sheng-Nan Sun,[a] Li-Ling He,[a] Qing Huang,[b] Jiang Liu *[a] and Ya-Qian Lan [a]

A ferrocene-modified COF, namely Ni-Tph-COF-Fc, was synthesized and applied in OER. Compared with Ni-Tph-COF-OH, Ni-Tph-COF-Fc shows improved performance with a current density of 99.6 mA cm^{-2}, an overpotential of 450 mV, and a Tafel slope of 73.1 mV dec^{-1}, which may be attributed to a synergy between introduced ferrocene and metalloporphyrin in the COFs. Moreover, the enhanced OER performance leads to an improved CO_2RR performance with an FE_{CO} of 93.1%. This work represents an effective strategy to enhance the anodic OER performance and realize efficient CO_2RR.

In recent years, various electrocatalysts have been developed for achieving highly efficient CO_2 reduction reaction (CO_2RR) and demonstrated great potential for practical applications.[1] However, most studies have focused only on the CO_2RR half-reaction at the cathode when evaluating the performance of conventional CO_2RR, while ignoring the anodic oxygen evolution reaction (OER), leading to a huge waste of energy.[2,3] OER with slow kinetics and unfavorable thermodynamics involves a four-electron-transfer process and the formation of an oxygen double bond, which has a high overpotential that requires high energy input. At the same time, slow OER leads to a restricted charge transfer equilibrium in the electrochemical system, which in turn affects the CO_2RR kinetics.[4,5] To overcome this problem, efficient OER electrocatalysts need to be introduced.

Covalent organic frameworks (COFs), as framework materials with well-defined atomic structures and tunable coordination environments, are potential platforms for catalytic reactions.[6–10] Their excellent structural designability and high stability are beneficial for probing the reaction mechanism of the OER and thus establishing the structure–activity relationship of catalysts.[11,12] Some of the building blocks in the structure of COFs have suitable coordination sites, which enable them to introduce metal active sites for typical catalytic reactions.[13,14] In addition, utilizing post-modification, COFs can precisely introduce multiple active sites with different chemical environments or be endowed with additional properties, such as higher electrical conductivity (a key factor for rapid electron transfer in electrocatalytic reactions).[15,16] At present, some COFs have been reported for OER.[17] However, insufficient electron-donor capacity results in some COFs not realizing their full potential as efficient electrocatalysts. Several pioneering studies have integrated electron-rich units (*e.g.*, polyoxometalate) into MOFs to significantly improve electrocatalytic performance.[18,19] Utilizing this strategy to construct novel framework materials with features such as multiple active sites or continuous electron transfer channels is essential to advance the electrocatalytic process. Ferrocene (Fc) is a highly stable and electron-rich system and has been proven to be an ideal electron-donating or electron-carrying unit.[20–22] When Fc is injected into the skeletons of COFs, it can serve as a potential electron donor or carrier to enhance the electron density of the COFs. To match the nature of Fc, the selected COFs should have the ability to carry or accept electrons. Metalloporphyrin-based COFs are considered to be highly promising candidates, in which the porphyrin ring is regarded as an ideal carrier to transfer charge, and the metal coordinated to the porphyrin ring can serve as an efficient electron acceptor and active catalytic site.[23,24] The combination of Fc and metalloporphyrin in the COFs can form electron transfer channels, which can drastically increase the electron transfer capacity and catalytic activity.

Herein, 1-bromoferrocene (Fc-Br) was chosen to post-modify the porphyrin-based COF (Ni-Tph-COF-OH) by a solvent-thermal method. Compared with Ni-Tph-COF-OH, the as-synthesized Ni-Tph-COF-Fc shows superior OER activity with a current density of 99.6 mA cm^{-2} at 2 V *vs.* RHE, which is 4.3 times higher than that of Ni-Tph-COF-OH. At 10 mA cm^{-2} current density, the overpotential of Ni-Tph-COF-Fc (450 mV) is lower than that of Ni-Tph-COF-OH (540 mV). In addition, the Tafel slope of Ni-Tph-COF-Fc is only 73.1 mV dec^{-1}. Comparative experiments show that the introduced Fc improves the electrical conductivity of the catalysts,

[a] *School of Chemistry, South China Normal University, Guangzhou, 510006, China. E-mail: liuj0828@m.scnu.edu.cn*
[b] *College of Materials Science and Engineering, Nanjing Forestry University, Nanjing, 210037, China*

† Electronic supplementary information (ESI) available. See DOI: https://doi.org/10.1039/d4cc02651a

Published on 05 July 2024. Downloaded by Zhejiang University on 7/17/2024 9:55:18 AM.

facilitates charge transfer during the electrochemical process, and provides more active sites, which enhances the OER performance of the catalysts. Notably, the enhanced anodic OER performance promotes the cathodic CO_2RR, and the FE_{CO} for the Ni-Tph-COF-Fc || Ni-Tph-COF-OH electrocatalytic system was higher than that for the Ni-Tph-COF-OH || Ni-Tph-COF-OH over the potential range from −0.8 V to −1.1 V with the FE_{CO} up to 93.1% at −0.9 V.

Ni-Tph-COF-OH was synthesized by a solvothermal method based on the Schiff base reaction between 2, 5-dihydroxy-1, 4-benzenedicarboxaldehyde (Dha) and 5, 10, 15, 20-tetrakis(4-aminophenyl)-21*H*, 23*H*-porphine (TAPP) according to the reported literature.[25] Then, the mixture of Ni-Tph-COF-OH and Fc-Br was refluxed in a mixed solvent of 1, 4-dioxane and Et_3N *via* nucleophilic substitution reaction to produce Ni-Tph-COF-Fc. For Ni-Tph-COF-OH, it is a porous two-dimensional (2D) COF formed by covalent bonding, with a pore size of about 2 nm and a theoretical distance of about 4 Å between the layers in the stacked structure (Fig. 1a and Fig. S1, ESI†). It is worth noting that the –OH groups in Ni-Tph-COF-OH allow the modification with other functional units (eg., Fc-Br) to produce the COF with a rapid electronic transfer system and rich catalytic active sites. The PXRD patterns in Fig. 1b show that the peaks of the as-synthesized Ni-Tph-COF-OH and Ni-Tph-COF-Fc are in agreement with the diffraction peaks obtained by the simulated one, which indicates that Ni-Tph-COF-Fc retains good crystallinity after modification and have high phase purity. In addition, the FT-IR and XPS were conducted to demonstrate the formation of covalent bonds in Ni-Tph-COF-Fc after modification. Compared with the FT-IR spectrum of TAPP, in the FT-IR spectrum of Ni-Tph-COF-OH, the disappearance of the peak corresponding to N–H stretching vibration at 3315 cm^{-1} and the appearance of a new peak at 999 cm^{-1} indicate that the porphyrin is coordinated to the metal (Fig. 1c). Moreover, the new peak ascribed to C═N stretching vibration appears at 1613 cm^{-1} in the FT-IR spectrum of Ni-Tph-COF-OH, proving the formation of Ni-Tph-COF-OH. Notably, the C═N stretching vibration band at 1613 cm^{-1} is still retained in the FT-IR spectrum of Ni-Tph-COF-Fc after the modification, and the characteristic peaks of Fc appear at 3098 and 479 cm^{-1}, respectively, which indicates the high stability of the COF during the modification process, and also proves that the presence of Fc in the structure of Ni-Tph-COF-Fc (Fig. 1c). As displayed in Fig. 1d, it can be found that the presence of C–O bond in the X-ray photoelectron spectroscopy (XPS) spectrum, which further confirms that the COF is successfully modified with Fc *via* C–O covalent bonds.[26,27] N_2 adsorption–desorption curves were obtained at 77.3 K to evaluate the structural porosity and specific surface area of these COFs. The results show that the pore size of Ni-Tph-COF-OH and Ni-Tph-COF-Fc are about 2 nm, which is consistent with the theoretical results (Fig. S2 and S3, ESI†). The Brunauer–Emmett–Teller (BET) surface area of Ni-Tph-COF-OH is 619 $cm^2\ g^{-1}$, whereas the BET surface area of Ni-Tph-COF-Fc is 214 $cm^2\ g^{-1}$. This discrepancy indicates that some of the pore channels of Ni-Tph-COF-Fc are occupied by Fc after the modification, which further confirms that Fc is successfully modified into the backbone of COF.

The morphologies of Ni-Tph-COF-Fc and Ni-Tph-COF-OH were characterized by SEM and TEM. The results show that both Ni-Tph-COF-Fc and Ni-Tph-COF-OH exhibit a nanosheet morphology (Fig. 2a, b and Fig. S4a, ESI†). The structural characteristics of Ni-Tph-COF-Fc and Ni-Tph-COF-OH were further observed through HR-TEM. As shown in Fig. 2c and Fig. S4b (ESI†), oriented lattice fringes with lattice spacing of 2.2 nm and 2.3 nm can be observed in the HR-TEM images of Ni-Tph-COF-Fc and Ni-Tph-COF-OH, respectively, which further confirms that the obtained Ni-Tph-COF-Fc and Ni-Tph-COF-OH have high crystallinity. Furthermore, energy dispersive X-ray spectroscopy (EDX) analysis shows that C, N, O, Ni, and Fe are uniformly distributed on Ni-Tph-COF-Fc (Fig. 2d and e), confirming the presence of Fe element in the Ni-Tph-COF-Fc and further proving that Fc is successfully modified into COF. In addition, EDX also shows that C, N, O, and Ni are uniformly distributed on Ni Tph-COF-OH (Fig. S5, ESI†). Similarly, other as-synthesized contrast samples were also characterized and the results are shown in ESI† (Fig. S6–S9).

Thermogravimetric analysis (TGA) tests were conducted under the O_2 atmosphere. As shown in Fig. S10 and S11 (ESI†), Ni-Tph-COF-Fc and Ni-Tph-COF-OH can be maximally stabilized

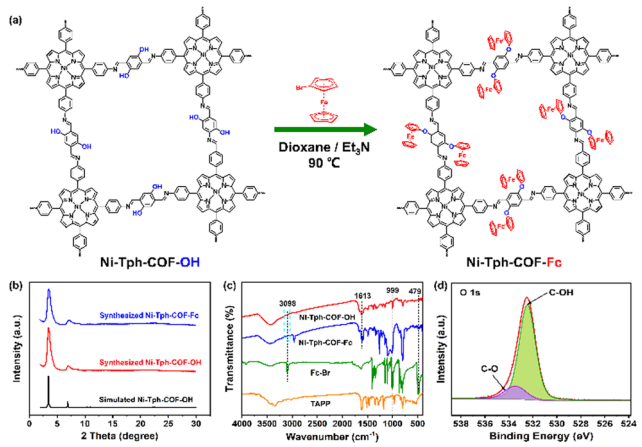

Fig. 1 The structure and physical characterization of Ni-Tph-COF-Fc. (a) Preparation process of Ni-Tph-COF-Fc. (b) The PXRD patterns. (c) FT-IR spectra. (d) XPS spectrum of Ni-Tph-COF-Fc.

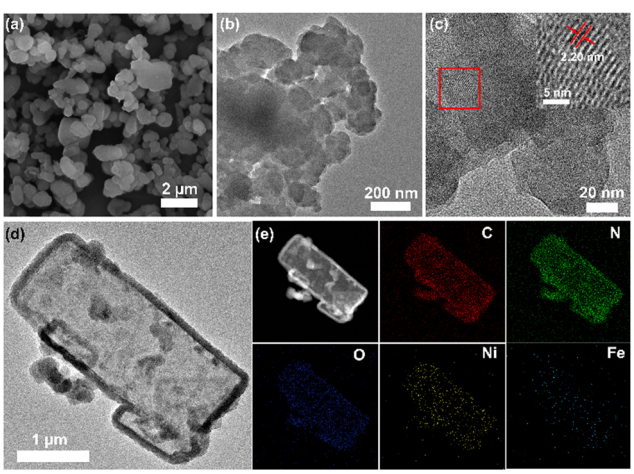

Fig. 2 Electron microscopic characterization of Ni-Tph-COF-Fc. (a) SEM. (b) TEM. (c) HR-TEM. (d) and (e) TEM and mapping images.

This journal is © The Royal Society of Chemistry 2024

Published on 05 July 2024. Downloaded by Zhejiang University on 7/17/2024 9:55:18 AM.

up to about 350 °C. To evaluate the chemical stability of the samples, the synthesized Ni-Tph-COF-OH was immersed in 1 M KOH and 0.5 M $KHCO_3$ aqueous solutions for 12 hours, after which the samples were filtered out for PXRD testing. As shown in Fig. S12 (ESI†), the PXRD peaks of the immersed samples remained consistent with the diffraction peaks of simulated PXRD, indicating that Ni-Tph-COF-OH can maintain structural integrity. Thus, Ni-Tph-COF-OH exhibits good thermal and chemical stability, which provides a good experimental basis for further investigation of the electrochemical activity of the materials.

The OER performance of Ni-Tph-COF-Fc was evaluated in a sealed H-type cell with 1 M KOH aqueous solution as electrolyte. The polarization curves displayed in Fig. 3a show that Ni-Tph-COF-Fc has a higher current density than Ni-Tph-COF-OH. At 2 V *vs.* RHE, Ni-Tph-COF-Fc can reach a current density of 99.6 mA cm^{-2}, which is about 4.3 times more than Ni-Tph-COF-OH (23.25 mA cm^{-2}). In addition, Ni-Tph-COF-Fc can reach a current density of 1 mA cm^{-2} at 1.6 V, which is 40 mV different from Ni-Tph-COF-OH (1.64 V). Tafel plots were calculated based on the polarization curves to analyze the kinetic process. The results show that the Tafel slopes of Ni-Tph-COF-Fc and Ni-Tph-COF-OH are 73.1 and 108.3 mV dec^{-1}, respectively, suggesting that Ni-Tph-COF-Fc shows a more favorable kinetics (Fig. 3b). η_{10} denotes the overpotential achieved at the current density of 10 mA cm^{-2}, which is an important parameter to evaluate the OER performance of the electrocatalysts. As shown in Fig. 3c, the η_{10} of Ni-Tph-COF-Fc is 450 mV, which is lower than that of Ni-Tph-COF-OH (540 mV). To shed further light on the OER performance of Ni-Tph-COF-Fc, the cyclic voltammogram (CV) curves were recorded to calculate the electrochemical double-layer capacitance (C_{dl}) and further estimate the electrochemically active surface area (ECSA) (Fig. S13, ESI†). Fig. 3d shows that the C_{dl} of Ni-Tph-COF-Fc (1.97 mF cm^{-2}) is higher than that of Ni-Tph-COF-OH (1.77 mF cm^{-2}), implying Ni-Tph-COF-Fc can provide more accessible surface and faster reaction rate during the OER process. Besides, the charge transfer resistance was evaluated by electrochemical impedance spectroscopy (EIS). The charge transfer resistance of Ni-Tph-COF-Fc is smaller than that of Ni-Tph-COF-OH, indicating that the shuttle of charge transfer on Ni-Tph-COF-Fc is faster in the OER process (Fig. S14, ESI†).

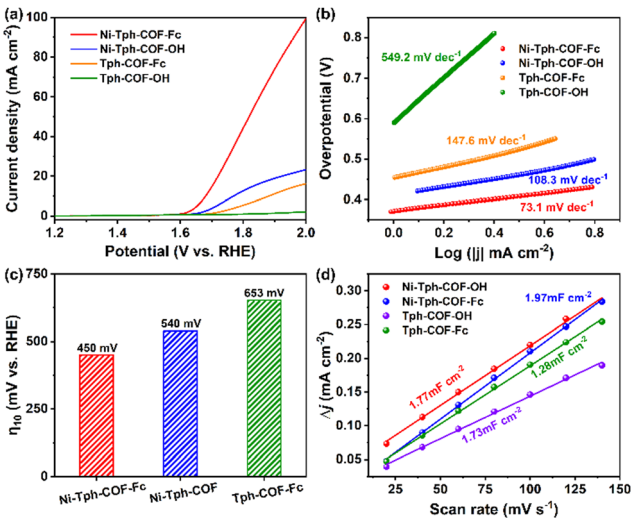

Fig. 3 The electrochemical performance of electrocatalysts. (a) Polarization curves of OER with different catalysts. (b) Tafel slopes. (c) Overpotential at a current density of 10 mA cm^{-2}. (d) C_{dl} of electrocatalysts.

To show the enhancement of catalytic performance of the catalyst by Fc more distinctly, the samples Tph-COF-OH and Tph-COF-Fc were synthesized to exclude the effect of metal Ni coordinated to porphyrin on the OER performance. As shown in Fig. 3a, the Fc-modified COF, Tph-COF-Fc, exhibits a significantly larger current density value of 16.1 mA cm^{-2} than Tph-COF-OH (2.1 mA cm^{-2}) at 2 V. Besides, at a current density of 1 mA cm^{-2}, the overpotential of Tph-COF-Fc is smaller than that of Tph-COF-OH by 134 mV. Moreover, the Tafel slope of Tph-COF-Fc (147.6 mV dec^{-1}) is much smaller than that of Tph-COF-OH (549.2 mV dec^{-1}), suggesting that the addition of Fc improves the reaction kinetics of the catalyst. The comparison of C_{dl} values in Fig. 3d shows that Tph-COF-Fc has a larger ECSA than Tph-COF-OH. All these experimental results indicate that Fc plays an important role in the OER performance of catalysts. Further comparing the OER performance of Ni-Tph-COF-Fc, Ni-Tph-COF-OH, Tph-COF-Fc, and Tph-COF-OH, it can be found that the catalyst with both the metal Ni and Fc shows the most excellent OER activity, which suggests the Fc and Ni synergistically in electrochemical OER (Fig. 3a). Additionally, CP (catalyst carrier) shows extremely poor OER performance, indicating that the good OER performance exhibited in the test indeed originated from the synthesized catalysts (Fig. S15, ESI†). The long-term stability for OER was assessed with a chronopotentiometric curve, which remains unchanged without degradation up to about 9 hours (Fig. S16, ESI†). Besides, the effect of different feedings of ferrocene during the synthesis process on the properties of the post-modified samples was studied. The synthesized samples are denoted as Ni-Tph-COF-2 (12 mg) and Ni-Tph-COF-3 (48 mg), respectively. PXRD patterns show that the diffraction peaks of the synthesized samples are similar to that of the simulated sample, which illustrates the good crystallinity of the materials (Fig. S17a, ESI†). The OER test results in Fig. S17b (ESI†) show that the current densities of Ni-Tph-COF-2 and Ni-Tph-COF-3 at 2 V *vs.* RHE potentials were 42.3 mA cm^{-2} and 45.9 mA cm^{-2}, respectively, which are much smaller than that of Ni-Tph-COF-Fc (99.6 mA cm^{-2}). Moreover, the onset potentials of both Ni-Tph-COF-2 and Ni-Tph-COF-3 are larger than that of Ni-Tph-COF-Fc. These results indicate that Ni-Tph-COF-Fc is the best modified sample.

Based on the OER performance, the CO_2RR performance of Ni-Tph-COF-Fc || Ni-Tph-COF-OH (Ni-Tph-COF-Fc at the anode and Ni-Tph-COF-OH at the cathode) and Ni-Tph-COF-OH || Ni-Tph-COF-OH were measured. As shown in Fig. 4a, the larger current density of Ni-Tph-COF-OH under a CO_2 atmosphere in the potential range of 0 V to −1.15 V indicates that Ni-Tph-COF-OH was more inclined to undergo the CO_2RR compared to HER in this interval. The performance of CO_2RR of Ni-Tph-COF-OH was further evaluated by controlled potential electrolysis. The gas-phase products and liquid-phase products produced by CO_2RR were detected by GC and ^{1}H-NMR, respectively. Fig. S18–S21 (ESI†) show that CO and H_2 are the gas-phase products of CO_2RR. The FE_{CO} of Ni-Tph-COF-OH || Ni-Tph-COF-OH shows a volcano-type curve in the

Published on 05 July 2024. Downloaded by Zhejiang University on 7/17/2024 9:55:18 AM.

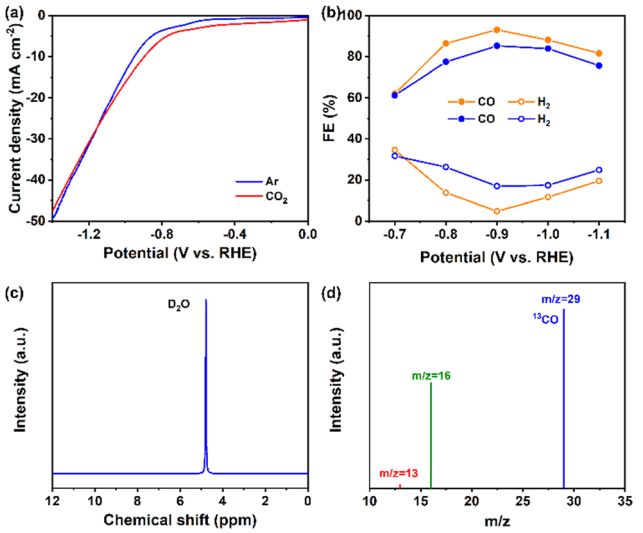

Fig. 4 The CO_2RR performance. (a) LSV curves of Ni-Tph-COF-OH under different atmospheres. (b) Faraday efficiency (blue line represents the Faraday efficiency of Ni-Tph-COF-OH || Ni-Tph-COF-OH, orange line represents the Faraday efficiency of Ni-Tph-COF-Fc || Ni-Tph-COF-OH). (c) ^{1}H-NMR. (d) Mass spectrum of ^{13}CO.

potential range of −0.7 V to −1.1 V and the FE_{CO} reaches its maximum value (85.2%) at −0.9 V (Fig. 4b). In contrast, it is obvious that Ni-Tph-COF-Fc || Ni-Tph-COF-OH exhibits better CO_2RR performance in the potential range of −0.8 V to −1.1 V, the FE_{CO} can even up to 93.1% at −0.9 V. Moreover, the CO_2RR performance in the two-electrode configuration was also measured and the result is similar to that in the three-electrode configuration (Fig. S22, ESI†). The improved CO_2RR performance may be attributed to the improved anodic OER performance. The comparative experiment demonstrates that the catalytic effect indeed originates from the synthesized catalysts (Fig. S23 and S24, ESI†). In addition, only the peak of D_2O is shown in the ^{1}H-NMR spectrum, which indicates that there is no liquid-phase product generated during the CO_2RR process (Fig. 4c). The isotope experiment was conducted and verified that the CO detected in the CO_2RR process was obtained from CO_2 (Fig. 4d).

In conclusion, a porphyrin-based COF modified with Fc (Ni-Tph-COF-Fc) was synthesized to study its OER performance. The synergistic effect between the introduced electron-rich group Fc and metalloporphyrin provides a continuous electron transfer channel in the COFs during the OER process, thus giving the catalyst excellent OER performance. Ni-Tph-COF-Fc shows a low Tafel slope of 73.1 mV dec^{-1} and can reach a current density of 99.6 mA cm^{-2} at 2 V, which is 4.3 times higher than that of Ni-Tph-COF-OH. Moreover, the η_{10} of Ni-Tph-COF-Fc (450 mV) is lower than that of Ni-Tph-COF-OH (540 mV). Notably, the enhanced OER performance promotes the cathodic CO_2RR performance. FE_{CO} of the Ni-Tph-COF-Fc || Ni-Tph-COF-OH electrocatalytic system can be boosted to 93.1%. Our research as a well-defined model system provides an effective strategy to enhance the anodic OER performance and opens a new way to realize efficient CO_2RR.

This work was financially supported by the NSFC (no. 22271104, 22225109, 22071109, and 22101089) and Guangdong Basic and Applied Basic Research Foundation (no. 2023B1515120060). The Top Youth Project of Guangdong Pearl River Talents Program (no. 2021QN02L617).

Data availability

The data supporting this article have been included as part of the ESI.†

Conflicts of interest

There are no conflicts to declare.

Notes and references

1 L.-L. Ling, L. Jiao, X. Liu, Y. Dong, W. Yang, H. Zhang, B. Ye, J. Chen and H.-L. Jiang, *Adv. Mater.*, 2022, **34**, 2205933.
2 R. Li, K. Xiang, Z. Peng, Y. Zou and S. Wang, *Adv. Energy Mater.*, 2021, **11**, 2102292.
3 J. Wang, X. Li, M. Wang, T. Zhang, X. Chai, J. Lu, T. Wang, Y. Zhao and D. Ma, *ACS Catal.*, 2022, **12**, 6722–6728.
4 W. Lai, Y. Qiao, J. Zhang, Z. Lin and H. Huang, *Energy Environ. Sci.*, 2022, **15**, 3603–3629.
5 Á. Vass, A. Kormányos, Z. Kószó, B. Endrődi and C. Janáky, *ACS Catal.*, 2022, **12**, 1037–1051.
6 K. Hou, H. Gu, Y. Yang, S. S. Lam, H. Li, C. Sonne, H. Ouyang and X. Chen, *Adv. Compos. Hybrid Mater.*, 2023, **6**, 199.
7 S. P. Teong and Y. Zhang, *ChemNanoMat*, 2023, **9**, e202300263.
8 Q. N. Tran, H. J. Lee and N. Tran, *Polymers*, 2023, **15**, 1279.
9 S. Daliran, M. Blanco, A. Dhakshinamoorthy, A. R. Oveisi, J. Alemán and H. García, *Adv. Funct. Mater.*, 2024, **34**, 2312912.
10 Q.-J. Wu, D.-H. Si, Q. Wu, Y.-L. Dong, R. Cao and Y.-B. Huang, *Angew. Chem., Int. Ed.*, 2023, **62**, e202215687.
11 Y. Yusran, X. Guan, H. Li, Q. Fang and S. Qiu, *Natl. Sci. Rev.*, 2020, **7**, 170–190.
12 N. Lv, Q. Li, H. Zhu, S. Mu, X. Luo, X. Ren, X. Liu, S. Li, C. Cheng and T. Ma, *Adv. Sci.*, 2023, **10**, 2206239.
13 L. Xiao, L. Qi, J. Sun, A. Husile, S. Zhang, Z. Wang and J. Guan, *Nano Energy*, 2024, **120**, 109155.
14 S. Huang, S. Lu, Y. Hu, Y. Cao, Y. Li, F. Duan, H. Zhu, Y. Jin, M. Du and W. Zhang, *Small Struct.*, 2023, **4**, 2200387.
15 M. Liu, S. Yang, X. Yang, C.-X. Cui, G. Liu, X. Li, J. He, G. Z. Chen, Q. Xu and G. Zeng, *Nat. Commun.*, 2023, **14**, 3800.
16 N. A. Rejali, M. Dinari and Y. Wang, *Chem. Commun.*, 2023, **59**, 11631–11647.
17 Z. Liang, H.-Y. Wang, H. Zheng, W. Zhang and R. Cao, *Chem. Soc. Rev.*, 2021, **50**, 2540–2581.
18 Y.-R. Wang, Q. Huang, C.-T. He, Y. Chen, J. Liu, F.-C. Shen and Y.-Q. Lan, *Nat. Commun.*, 2018, **9**, 4466.
19 M.-L. Sun, Y.-R. Wang, W.-W. He, R.-L. Zhong, Q.-Z. Liu, S. Xu, J.-M. Xu, X.-L. Han, X. Ge, S.-L. Li, Y.-Q. Lan, A. M. Al-Enizi, A. Nafady and S. Ma, *Small*, 2021, **17**, 2100762.
20 Z. Xin, Y.-R. Wang, Y. Chen, W.-L. Li, L.-Z. Dong and Y.-Q. Lan, *Nano Energy*, 2020, **67**, 104233.
21 H. Atzkern, B. Huber, F. H. Koehler, G. Mueller and R. Mueller, *Organometallics*, 1991, **10**, 238–244.
22 G.-Q. Lai, N. Li, J. He and Y.-Q. Lan, *Chem. Commun.*, 2023, **59**, 12471–12474.
23 Y.-C. Feng, X. Wang and D. Wang, *Mater. Chem. Front.*, 2024, **8**, 228–247.
24 Q.-J. Wu, D.-H. Si, S. Ye, Y.-L. Dong, R. Cao and Y.-B. Huang, *J. Am. Chem. Soc.*, 2023, **145**, 19856–19865.
25 B. Cheng, Y. Zhong, Y. Qiu, S. Vaikuntanathan and J. Park, *J. Am. Chem. Soc.*, 2023, **145**, 5261–5269.
26 Y.-J. Tang, C.-H. Liu, W. Huang, X.-L. Wang, L.-Z. Dong, S.-L. Li and Y.-Q. Lan, *ACS Appl. Mater. Interfaces*, 2017, **9**, 16977–16985.
27 F.-C. Shen, Y. Wang, Y.-J. Tang, S.-L. Li, Y.-R. Wang, L.-Z. Dong, Y.-F. Li, Y. Xu and Y.-Q. Lan, *ACS Energy Lett.*, 2017, **2**, 1327–1333.

 This journal is © The Royal Society of Chemistry 2024